Validation of diffuse reflectance spectroscopy with magnetic resonance imaging for accurate vertebral bone fat fraction quantification

Swamy, Akash; Burström, Gustav; Spliethoff, Jarich W.; Babic, Drazenko; Ruschke, Stefan; Racadio, John M.; Edström, Erik; Terander, Adrian Elmi; Dankelman, Jenny; Hendriks, Benno H.W.

DOI
10.1364/BOE.10.004316

Publication date
2019

Document Version
Final published version

Published in
Biomedical Optics Express

Research Article | Vol. 10, No. 8 | 1 Aug 2019 | BIOMEDICAL OPTICS EXPRESS 4316
Biomedical Optics EXPRESS

Validation of diffuse reflectance spectroscopy with magnetic resonance imaging for accurate vertebral bone fat fraction quantification

Akash Swamy,[1,2,*] Gustav Burström,[3] Jarich W. Spliethoff,[2] Drazenko Babic,[2] Stefan Ruschke,[4] John M. Racadio,[5] Erik Edström,[3] Adrian Elmi Terander,[3] Jenny Dankelman,[1] and Benno H. W. Hendriks[1,2]

[1]*Department of Biomechanical Engineering, Delft University of Technology, Mekelweg 2, 2628 CD, Delft, the Netherlands*
[2]*Department of In-body Systems, Philips Research, Royal Philips NV, High Tech Campus 34, 5656 AE, Eindhoven, the Netherlands*
[3]*Department of Clinical Neuroscience, Karolinska Institutet, Stockholm, Sweden and Department of Neurosurgery, Karolinska University Hospital, 17176, Stockholm, Sweden*
[4]*Department of Radiology, Klinikum rechts der Isar, Technical University of Munich, Ismaninger Straße 22, 81675 München, Germany*
[5]*Cincinnati Children's Hospital Medical Center, 3333 Burnet Avenue, Cincinnati, Ohio, USA*
**a.swamy@tudelft.nl*

Abstract: Safe and accurate placement of pedicle screws remains a critical step in open and minimally invasive spine surgery. The diffuse reflectance spectroscopy (DRS) technique may offer the possibility of intra-operative guidance for pedicle screw placement. Currently, Magnetic Resonance Imaging (MRI) is one of the most accurate techniques used to measure fat concentration in tissues. Therefore, the purpose of this study is to compare the accuracy of fat content measured invasively in vertebrae using DRS and validate it against the Proton density fat fraction (PDFF) derived via MRI. Chemical shift-encoding-based water-fat imaging of the spine was first performed on six cadavers. PDFF images were computed and manually segmented. 23 insertions using a custom-made screw probe with integrated optical fibers were then performed under cone beam computer tomography (CBCT). DR spectra were recorded at several positions along the trajectory as the optical screw probe was inserted turn by turn into the vertebral body. Fat fractions determined via DRS and MRI techniques were compared by spatially correlating the optical screw probe position within the vertebrae on CBCT images with respect to the PDFF images. The fat fraction determined by DRS was found to have a high correlation with those determined by MRI, with a Pearson coefficient of 0.950 ($P < 0.001$) as compared with PDFF measurements calculated from the MRI technique. Additionally, the two techniques were found to be comparable for fat fraction quantification within vertebral bodies ($R^2 = 0.905$).

1. Introduction

Spinal fusion surgeries are on the rise all over the world due to aging populations and a trend towards accepting elderly patients with increasingly complex medical histories [1,2]. During spinal fusion surgery, pedicle screws are commonly placed into the vertebrae to serve as anchoring points for rigid constructs, in order to fuse parts of the spine [3]. Inaccurate placement of pedicle screws could potentially lead to severe vascular and neurological injuries in patients [4–6]. Adding to the complexity of the procedure, minimally invasive surgeries (MIS) are rapidly increasing and might involve more than half of all spinal procedures by 2020 [7]. MIS procedures, significantly reduce blood loss, shorten hospital stay and decrease surgical site infections [8–13]. MIS is performed through a series of small

#366809 https://doi.org/10.1364/BOE.10.004316
Journal © 2019 Received 6 May 2019; revised 9 Jun 2019; accepted 11 Jun 2019; published 1 Aug 2019

Biomedical Optics EXPRESS

incisions, and requires guidance techniques to compensate for the limited visibility of important anatomical landmarks. There are several guidance techniques for accurate and safe pedicle screw placement. These include navigation systems and other non-imaging based techniques [14]. Pedicle screws could be placed by free-hand-technique or fluoroscopy-guided techniques, where the surgeon relies on experience, tactile feedback, and identifying anatomical landmarks. However, the accuracy rates of pedicle screw placement as reported in the literature are as low as 27.6% and as high as 96.5% based on a meta-analysis by Kosmopoulous et al. [15]. A more recent meta-analysis study found an accuracy range of 50-92% [16]. These inaccuracies translates into screw revisions being needed in 6.0% of operated patients, according to a recent systematic review by Staartjes et al. [17]. Therefore, there is a need for more reliable and cost-effective solutions for increasing the accuracy and safety in the placement of spinal screw implants during spinal fusion surgery.

Diffuse reflectance spectroscopy (DRS) may offer the possibility of intra-operative guidance of surgical instruments or implants by determining fat and water content in vertebral bone in real-time along the screw path. The quantification of fat content relative to water content from DR spectra or Diffuse Reflectance-based Fat Fraction (DRFF) has been studied extensively by previous researchers [18–21]. Previously, the DRS technique has been used for fat fraction quantification in tissue types such as liver and breast for early diagnosis of nonalcoholic fatty liver disease and tumor detection [21–23]. The use of a custom-made screw probe with integrated fiber-optics to perform image-guided insertions in an ex vivo (human) setting has previously been described [24]. The optical screw probe was inserted into the vertebrae and with each turn, the local fat content of the bone at the probe tip was measured in real-time. It was found that fat content was a good discriminator for cancellous and cortical bone. Moreover, the probe could be used to predict the transition between the two bone types and thereby potentially be used to prevent pedicle screws from breaching the cortical border [24].

A logical next step is to get a better understanding of the variation of DRFF within vertebrae of patients who undergo spinal fusion surgery, as this is pivotal in the development of a robust optical guidance technique for pedicle screw placement procedures.

Currently, Magnetic Resonance Spectroscopy (MRS) and Magnetic Resonance Imaging (MRI) are the most common techniques used to non-invasively measure fat concentration in vertebral bone tissues [25–36]. The quantitative assessment of fat fraction in vertebral bone has multiple clinical applications, including the characterization of bone health for evaluating conditions such as osteoporosis [28,33,34,37] diagnosis of metabolic disorders such as obesity and diabetes [32,38]; and cancer [39,40]. Proton density fat fraction (PDFF) is the de facto standardized MR-based biomarker for the determination of tissue fat concentration measured via MRI, and is considered to accurately reflect the concentration of fat in tissues [25,41]. Extensive clinical literature on PDFF measured non-invasively in vertebrae across patient cohorts of spinal fusion surgery, might help in providing crucial insights into the variation in DRFF measured along the optical screw path by the DRS technique. However, in order to do so, the DRFF would have to be benchmarked against the PDFF.

Therefore, the purpose of this study is to compare the accuracy of fat fraction measured invasively in vertebrae by the DRS technique (DRFF) and benchmark it to the PDFF parameter measured non-invasively via MRI.

2. Methods

2.1. Spinal tissues

A cadaver-based experiment was conducted at the Cincinnati Children's Hospital Medical Center, Ohio, United States. The donors allowed their bodies and body parts to be used for research and educational purposes. All ethical guidelines for human cadaver studies were followed. The characteristics of the studied cadavers (5 female, 1 male) are depicted in Table

Biomedical Optics EXPRESS

1. No embalming process was used, neither were any of the cadavers frozen, in order to preserve the optical properties of the cadaver specimens.

Table 1. Cadaver information.

Cadaver #	Gender	Age (years)	Weight (kg)[b]
1	Female	92	82
2	Female	82	77
3	Male	78	82
4	Female	53	77
5	Female [a]	79	68
6	Female	83	77

[a]Cause of death: malignant neoplasm. [b]Weights are estimates

2.2. Measurement protocol

2.2.1. Magnetic resonance imaging

The entire spine of the cadavers was scanned on a 1.5 Tesla (T) whole-body scanner (Ingenia, Philips Healthcare, Best, Netherlands) while placed in the prone position on the table coil array. To obtain whole spine coverage, the MR exam consisted of three sagittal 3D spoiled gradient echo sequences placed on the cervical, thoracic and lumbar spine, respectively. The temperature of the cadavers was maintained close to room temperature prior to scanning.

A three-dimensional (3D) six-echo spoiled gradient-echo sequence was used for chemical shift-encoding-based water-fat separation. The typical imaging parameters used in this study were: 45-60 sagittal slices with a slice thickness of 3 mm; AP and FH field of view = 220-310 and 240-350 mm; in-plane resolution = (0.45-0.67) × (0.45-0.67) mm; flip angle = 5 degrees; TR = 9.9-15.87 ms; TE1 = 1.41-1.43 ms; ΔTE = 1.2 ms; total scan time per cadaver was approximately 5-10 minutes.

2.2.2. Diffuse Reflectance spectroscopy

The DRS system consists of a tungsten halogen broadband light source (360 – 2500 nm) and optical spectrometers as shown in the schematic diagram of Fig. 1. The spectrometers collectively cover the visible, near-infrared and shortwave infrared wavelength range; the first spectrometer resolves light in the visible (Ocean Optics Maya2000Pro), while the second resolves light in the infrared wavelength range (Ocean Optics NirQuest), together resolving the light between 400 to 1600 nm. An in-house developed LabVIEW software (National Instruments, Austin, Texas) was used to control the spectrometers and acquire the data. The DRS system used in this study has been thoroughly described previously, along with the calibration procedure [19,20,42].

The custom-made optical screw probe (diameter: 5.5 mm) used to obtain DR spectra is illustrated in Fig. 1. The optical screw probe consisted of two optical fibers with core diameter of 200 µm. One of the fibers was used to transport the light from the source to the tissue, while the second fiber was used to transport the diffusely reflected light from the tissue to both spectrometers. The center-to-center distance between the collecting fiber and the delivering fiber was set at 1.22 mm as shown in Fig. 1. In previous work, a good trade-off was found between signal-to-noise ratio and probing depth based on a fiber-to-fiber distance of around 1.2 mm. The fiber distance was also chosen based on the largest penetration depth achievable, which was bounded by the optical screw probe diameter and manufacturing tolerances, in order to house the fibers in the screw.

Biomedical Optics EXPRESS

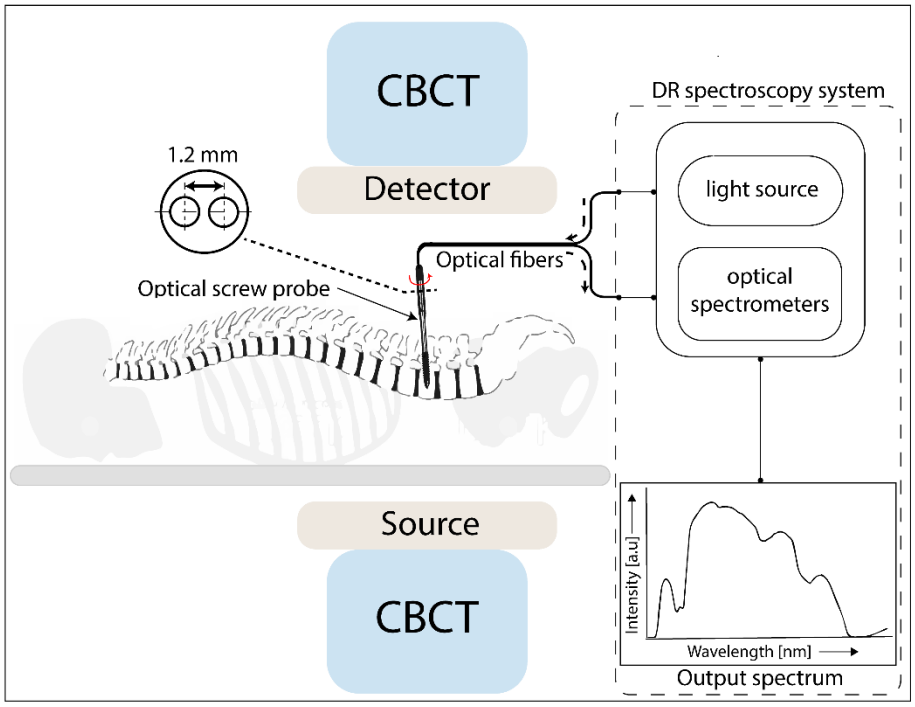

Fig. 1. Schematic of the experimental setup. Turn-by-turn insertion of the optical screw probe with DR output spectra recording performed by the DRS system under intraoperative cone beam computer tomography (CBCT) acquisitions.

After the MR exam, the cadavers were transferred to an operating table and placed in prone position. The spine was exposed using a midline approach. A total of 23 insertions were performed in six cadavers across levels ranging from cervical (C2) to lumbar (L5) using the optical screw probe. DR spectra were recorded at several positions along the trajectory, as the optical screw probe was inserted turn-by-turn into the vertebral body (Fig. 1). Five to ten DR spectra were acquired per turn. Subsequently, cone beam computer tomography (CBCT) images (AlluraClarity FD20; Philips Healthcare, Best, the Netherlands) were acquired at regular intervals based on the approximate probe positions within vertebral body. CBCT's were also acquired whenever a change in DRS readings were encountered to increase the likelihood of capturing all relevant positions within the vertebral body. The number of CBCT images acquired per insertion were 5-10.

2.3. Determination of fat fraction in vertebral bones

2.3.1. Proton density fat fraction

The scanner image reconstruction was utilized to obtain fat and water images using a DICOM image viewer software (Philips DICOM viewer R3.0-SP04, Philips Healthcare, Best, The Netherlands). The water—fat separation was based on a complex seven-peak water—fat spectral model. Based on the fat (F) and water images (W), PDFF was thus calculated as:

$$PDFF[\%] = \frac{F}{F+W} \times 100. \quad (1)$$

In order to validate the PDFF images for accurate fat fraction quantification, a phantom of known fat fraction values ranging from 0 to 100% (Calimetrix Fat fraction Phantom (Model 100), Sl no. F0008100) was scanned three times using the scatter settings mentioned above.

Biomedical Optics EXPRESS

The averaged PDFF measurements from multiple phantom scans were then compared to known fat fraction values of the phantom.

In order to calculate the anatomical variation of vertebral body PDFF distribution across all spinal levels, manual determination of the vertebral bone marrow fat fraction was performed by placing circular regions of interests (ROIs) on the PDFF map on three most central slices per vertebral level from C3 to L5. Each ROI was placed in the ventral half of the vertebrae, equidistant to both the endplates, and covering two-thirds of the vertebral body height.

2.3.2. Diffuse reflectance fat fraction

A modified version of the model developed by Farrell et al. [43] was used to extract tissue optical properties from the measured spectra. The absorption coefficient $\mu_a(\lambda)$ and reduced scattering coefficients $\mu_{s'}(\lambda)$ were extracted from the model expressed in cm^{-1}. From the known wavelength-dependent absorption coefficients and fiber distance between the emitting and collecting fibers, the amount of fat [%] and water [%] present in the tissue probed locally were determined following a procedure as previously described by the group [17,41]. DRFF was calculated as follows:

$$DRFF[\%] = \frac{Fat}{Fat + Water} \times 100. \quad (2)$$

2.4. Fat fraction correlation scheme between PDFF and DRFF determination

2.4.1. Vertebral body region correlation

In order to compare the DRFF and PDFF, the spatial location of the optical screw probe within the vertebral body was correlated with respect to CBCT images and PDFF images. First, a suitable image slice showing the location of the optical screw probe within the vertebral body was selected by a trained physician by toggling through the sagittal, axial and coronal slices of the CBCT data sets. A CBCT image showing the optical screw probe in a sagittal slice of one such insertion is shown in Fig. 2a. By identifying and matching anatomical landmarks and features in the CBCT image, the corresponding PDFF image was then selected. Manual determination of the vertebral bone marrow fat fraction was performed by placing circular regions of interests (ROIs) in the PDFF image as shown in Fig. 2b. The radius of the circular ROI was set between 2.7- 3.0 pixels. The ROI radius was calculated based on the approximate linear distance travelled by the optical screw probe due to 1-2 consecutive turns from the position found in the CBCT image. Thus, spatially correlating the PDFF pixels with DRFF probing volume. The average PDFF, standard deviation (SD), standard error (SE) from all pixels lying within the circular ROI were extracted and compared to DRS measurements.

2.5. Statistical analysis

The data obtained from each technique was tested using the Jarque-Bera test for normality [44] and was found to come from a normal distribution. Thus, the estimated fat fractions are calculated as mean ± SD and SE.

A one-sample t-test was applied to evaluate whether fat fraction obtained via DRS is significantly different from fat fraction obtained via MRI. Pearson correlation coefficient was used to assess the linearity in the estimated fat fraction determined by DRS as compared to PDFF values determined by MRI. Pairwise linear regression fits were also performed to assess the relation of fat fraction estimation between DRS and MRI. SE values were taken as weighing factor in the linear regression fits based on the maximum likelihood estimation statistical technique [45]. For each regression coefficient, a 95% confidence interval was also calculated.

Biomedical Optics EXPRESS

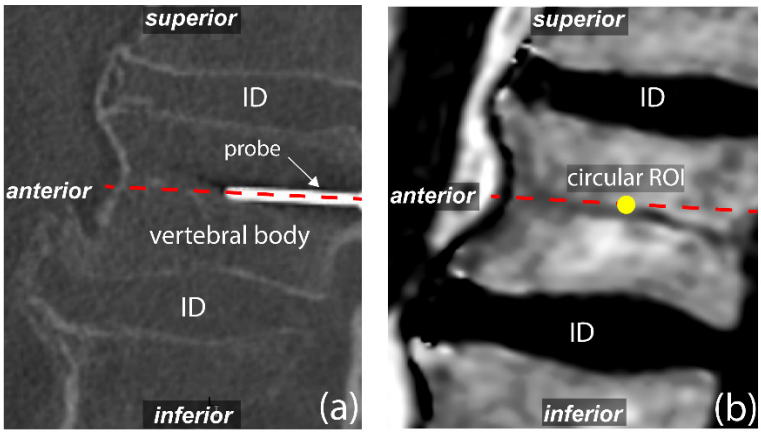

Fig. 2. (a). Sagittal slice showing optical screw probe within vertebral body. (b) MR image depicting circular ROI placement for PDFF extraction. Thick dashed line illustrates trajectory of optical screw probe. *ID = Intervertebral disc.

3. Results

3.1. Phantom fat fraction measurements

PDFF values calculated via MRI were found to be statistically similar to the known fat fraction values of the reference phantom (P = 0.187). MRI for PDFF quantification showed a very high correlation with Pearson coefficient above 0.990 (P<0.001), as compared to known reference phantom fat fraction measurements as depicted in Fig. 3.

3.2. Cadaver fat fraction measurements

Figure 4 shows the correlation of PDFF versus DRFF. The DRFF values were found to be statistically similar to the PDFF values (P = 0.969). DRFF was found to have high correlation with Pearson coefficient of 0.950 (P< 0.001) as compared to PDFF measurements. Additionally, based on the linear regression coefficient (R^2 = 0.905), the results of the two techniques were highly correlated.

Figure 5(a)-(f) illustrate the spatial variation of vertebral fat fraction along the spines of six cadavers studied according to the MRI measurements. PDFF averaged over cervical, thoracic and lumbar regions of the spine for all cadavers is given in Table 2.

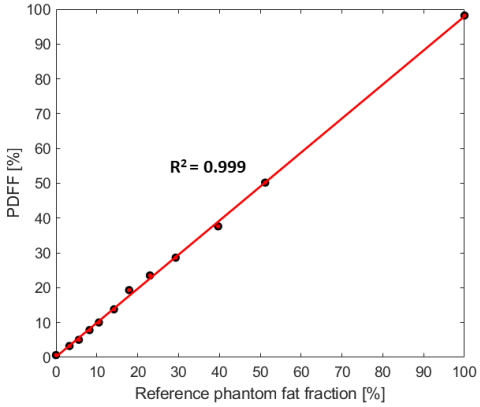

Fig. 3. Correlation plot depicting PDFF determined via MRI as compared to known phantom fat fraction measurements.

Biomedical Optics EXPRESS

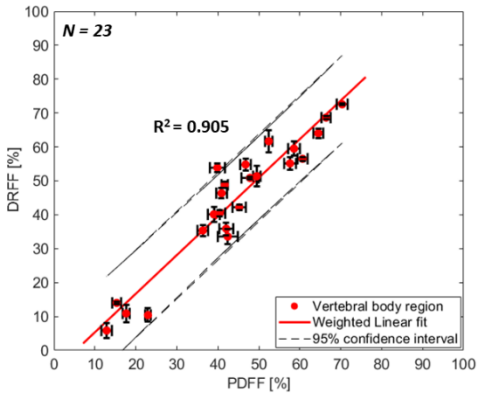

Fig. 4. Correlation plot depicting mean and standard error of fat fraction determined by DRS versus MRI Imaging. Correlation of fat fraction between two techniques in vertebral body region of the vertebrae. Error bars indicate SE.

4. Discussion

In the present study, we evaluated the measurements of fat fraction, determined by the DRS sensing technique during insertion of a custom-made optical screw probe into the vertebrae of six human cadavers. These measurements were compared with ex vivo MRI measurements, which is the clinically standardized technique for non-invasive fat fraction measurements in biological tissues [46].

Fat fraction quantification within vertebral body regions of the spine using the DRS technique, showed to be in good agreement with values obtained by MRI technique. The error bars arising from the fat fraction measurement via the MRI technique are a consequence of variation of fat fraction within the chosen region of interest on the PDFF images. The source of variation indicated by the error bars in Fig. 4 can be attributed to inherent heterogeneities within vertebrae especially due to random distribution of triglyceride (fat) storage sites within the trabecular structure of cancellous bone [47]. The source of variation in DRFF can also be linked to the inherent heterogeneities of vertebral bone samples since, each DRS mean and SE value is based on two to three unique measurement positions of the probe tip within the bone. Uncertainties also arise from the assumptions made by the Farrell model used to quantify fat fraction from the DRS signal [19].

It is worth noting that there is a fundamental difference between how fat fraction is determined via the MRI and DRS technique. The MR signal and assumed signal model reflects a tissue property referred to as proton density. It aims for the proton density of only triglycerides and water, respectively. Whereas, the DR signal model reflects the tissue property based on the interactions of photons within the finite volume of tissue probed locally. Although PDFF is capturing a fundamentally different property as compared to DRFF, the measured properties should highly correlate with each other as they attempt to measure similar tissue properties.

The PDFF distribution within the vertebral body across L1-L5 lumbar levels of the spine was found in the range of 40 – 62% across all cadavers with an exception of cadaver 5 (Fig. 5a-f). These cadavers had a mean age of 78 years (Table 1). Cadavers studied in the ex vivo setting in this study belonged to the older adults patient cohort. This patient cohort is the most common cohort for spinal surgery, suffering from back pain due to a wide variety of indications including degenerative disorders such as degenerative disc disease, spinal stenosis, spondylolysis, spondylolisthesis [48] and vertebral fractures [49].

Biomedical Optics EXPRESS

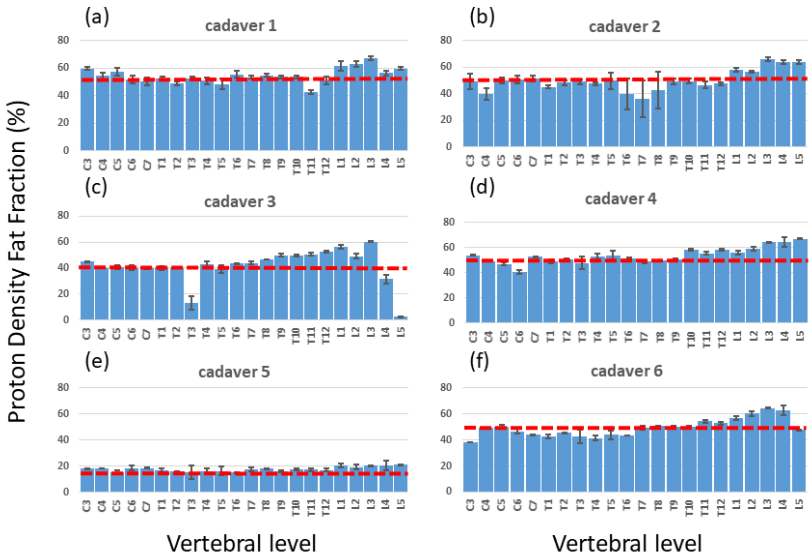

Fig. 5. Anatomical variation of vertebral body PDFF across whole spines of six cadavers. The dotted line represents the mean fat fraction across cervical to lumbar vertebral levels.

Table 2. Mean ± SD of vertebral body region PDFF averaged over cervical, thoracic and lumbar vertebral levels according to MRI measurements.

Levels	Cadaver 1	Cadaver 2	Cadaver 3	Cadaver 4	Cadaver 5	Cadaver 6
C3-C7	54.7 ± 3.9%	48.2 ± 4.9%	41.2 ± 2.2%	48.7 ± 5.3%	17.7 ± 1.4%	45.6 ± 4.8%
T1-T6	51.4 ± 2.7%	46.5 ± 3.7%	36.6 ± 11.6%	51.0 ± 2.3%	15.9 ± 0.6%	43.4 ± 1.3%
T7-T12	51.5 ± 4.6%	45.3 ± 5.1%	48.8 ± 3.1%	53.4 ± 4.3%	17.2 ± 0.7%	51.3 ± 1.9%
L1-L5	61.4 ± 3.9%	61.7 ± 4.2%	39.9 ± 23.6%	62.1 ± 4.4%	20.2 ± 0.6%	58.4 ± 6.7%
All levels	54.5 ± 5.4%	50.0 ± 7.8%	41.7 ± 12.8%	53.6 ± 6.3%	17.6 ± 1.8%	49.5 ± 6.9%

Kuhn et al. [50] measured the PDFF of 51 men and women (mean age = 69.7 ± 9 years) from four levels (L1-L4) and found the average PDFF to be equal to 57.7 ± 14.4% in all patients. Patients whose vertebral bodies were osteoporotic had a significantly higher PDFF (mean PDFF = 62.4 ± 11%) compared to patients with healthy vertebrae (mean PDFF = 56.3 ± 14.8%). A similar study conducted by the group of Yeung et al. [51] found the same ball park of PDFF between healthy and osteoporotic patients. Schwartz et al. [52] measured bone marrow fat in an Icelandic population, from four vertebral levels (L1-L4) of 257 men and women (mean age = 79 ± 3.1 years), using the MRS technique. They found the mean fat fraction to be equal to 53.5% ± 8.1% in men and 55.0% ± 8.4% in women.

The PDFF measured non-invasively in these older patient cohorts' indicate differences in fat content in vertebrae due to gender and diseases such as osteoporosis. However, the range of PDFF measured in these patients in an in vivo setting were found to lie within the range of 40-62% of PDFF measured in the ex vivo human setting in this study.

Cadaver5 was found to have lower PDFF compared to the rest of the cadavers studied. The patient was found to suffer from malignant neoplasm of the esophagus, which might have been the cause of the low PDFF found across all spinal levels. Patients with active malignancy would have a higher chance of perioperative complications [53] and would be less likely to be considered for spinal fusion surgery. Still, in cases of malignances, the DRS technique needs to be further investigated before its use in a clinical setting.

Cadaver3 was found to have low fat fraction within the vertebral body of T3, L4 and L5 (Fig. 5c) using the method described in this study. It should be noted, however, that these vertebrae showed a clear pathology and altered anatomy based on water and fat MRI images.

Biomedical Optics EXPRESS

Thus, the measurements were most likely not representative of vertebral body tissue at all. Possible reasons for this could be an underlying malignancy or posterior vertebral scalloping, an effect of a multitude of different conditions including dural ectasia and intraspinal tumors deforming the vertebra [54].

Another patient cohort who undergoes spinal fusion surgery are adolescents suffering from spinal deformities. Adolescent Idiopathic Scoliosis (AIS) is a structural three-dimensional deformity of the spine that affects children during puberty [55]. In cases of severe deformity, surgical intervention is needed and typically involves instrumentation at multiple vertebral levels in both the thoracic and lumbar spine. None of the cadavers in this study belonged to this patient cohort. However, Ruschke et al. [56] measured the PDFF of 93 otherwise healthy children whose ages ranged between 9 and 18 years. They found the variation of PDFF in this patient cohort to be between 19% (at C3) and 40% (at L5) with a mean PDFF of 33.8%.

Therefore, based on in vivo human PDFF measurements across these MR studies, variation of fat fraction due to age, gender, vertebral levels and diseases exists [30,56,57]. Moreover, variations of fat fraction across the two patient cohorts', older adults and adolescents also exists.

Exploring the performance of DRS closer to the cortical bone than was measured in this study would be of interest for verifying it in the context of detecting the cortical border. However, such measurements introduce significant measurement inaccuracies when trying to correlate the position of probe in the CBCT (hence, the DRFF) to the precise location of cortical bone boundary ahead of probe in the PDFF image. Therefore, for the purpose of this study, we focused on correlating fat fraction values in areas where spatial correlation was less sensitive to errors. In future studies, it will therefore be of interest to further investigate the fat correlation close to or at the cortical border.

Our study had some limitations. Identification of the appropriate PDFF sagittal slice based on position of the optical screw probe within the bone from CBCT images was performed manually. An automated algorithm to fuse PDFF images with CBCT images in order to precisely match the probe position within the PDFF map might be a superior approach. Fat fraction maps were segmented manually. An automatic segmentation algorithm might be preferable. However, the method of fat fraction quantification via MRI was reproduced based on studies by previous researchers [30,56]. The assumed water-fat model for the calculation of PDFF does not correct for temperature shifts and may also be prone to potential model mismatches. However, the expected bias is expected to be low as the validation of PDFF measurements were performed using a calibration phantom.

Previously, Meritt et al. [58] used a combination of frequency-domain and steady-state optical spectroscopy system to compare the fat fraction with MRI on emulsion phantoms. They used a wavelength window of 650-1000 nm range and found a high correlation between the two techniques as well. Nachabe et al. [21] used an even wider wavelength window of 450-1800 nm for benchmarking the spectroscopy technique with MRS in liver of mice and found a high Pearson's correlation coefficient of 0.993. However, to the best of our knowledge this is the first study to validate the invasive DRS technique against the MRI technique in order to use fat fraction as a sensing parameter for instrument breach detection during spinal fusion surgery.

In our study, the distribution of fat fraction in the vertebral body across all vertebral levels was found to be in the range of 41.7-54.5% (Table 2) in the older adult cohort.

However, for the DRS technique to measure fat fraction along the screw path, the technique would have to accommodate for the variation in fat fraction within the vertebral body region due to age, gender, vertebral levels and comorbidities. These factors could be used as classification categories during the development of the breach detection algorithm. For instance, the apparent large differences in fat fraction ranges between older patient cohort and the young adolescent cohort should be taken into account by possibly adapting the fat

Biomedical Optics EXPRESS

fraction thresholding window manually or by incorporating artificially intelligent data-driven statistical techniques into the sensing algorithm. Moreover, in a previous study [23] we showed that apart from fat fraction, blood content and photon scattering might also be useful parameters for breach detection; however, further studies are required to strengthen this claim.

Successful adoption of the DRS technique into the surgical theatre depends on its clinical usefulness in relation to other currently used methods for improving accuracy. These methods include 3D navigation and robotics [59–62]. They have both been shown to improve accuracy and to decrease revision surgery rates compared to the free-hand technique. However, even though these technologies improve the accuracy there is still a remaining share of misplaced screws [17,63,64]. DRS would provide an additional, and different, approach to reducing the rate of misplaced screws. Where navigation and robotics improve spatial orientation, DRS would provide a warning that there was a tissue change. This means DRS implementation in surgical instruments could be an adjunct to other technologies to further increase accuracy. Where costs are of great importance, DRS could also prove to be a more cost-effective solution, compared to the large investments needed for navigation and robotics, as a stand-alone technical aid. Investigating the value of the DRS technique as a breach detection tool in the clinical environment will be part of future studies.

5. Conclusion

This study investigated the potential of DRS for fat fraction quantification in vertebrae. The technique was validated against a highly accurate non-invasive technique for fat fraction quantification namely MRI. Thus, we hypothesize that optical fibers integrated into a surgical instrument can accurately measure fat content within vertebrae and might therefore be used as a promising breach detection tool during pedicle screw placement procedures.

Funding

Philips Research.

Acknowledgements

The authors thank Diana M. Lindquist, Brynne Williams, Lacey Haas and Nicole Hilvert for their crucial insights during data acquisition and processing of the MRI data. The authors would also like to thank Christian Reich and Joanneke Groen for establishing the collaborations between various stakeholders during this multi-institutional study.

Disclosures

The authors who are affiliated with Philips Research (B.H.W.H., J.W.S., D.B.) only have financial interests in the subject matter, materials, and equipment, in the sense that they are an employee of Philips. None of the other authors have any financial relationship or conflict of interests.

References

1. S. T. Kha, H. Ilyas, J. E. Tanenbaum, E. C. Benzel, M. P. Steinmetz, and T. E. Mroz, "Trends in Lumbar Fusion Surgery Among Octogenarians: A Nationwide Inpatient Sample Study From 2004 to 2013," Global Spine J. **8**(6), 593–599 (2018).
2. K. Kobayashi, K. Ando, Y. Nishida, N. Ishiguro, and S. Imagama, "Epidemiological trends in spine surgery over 10 years in a multicenter database," Eur. Spine J. **27**(8), 1698–1703 (2018).
3. R. W. Gaines, Jr., "The use of pedicle-screw internal fixation for the operative treatment of spinal disorders," J. Bone Joint Surg. Am. **82**(10), 1458–1476 (2000).
4. L. Balabaud, S. Pitel, I. Caux, C. Dova, B. Richard, P. Antonietti, and C. Mazel, "Lumbar spine surgery in patients 80 years of age or older: morbidity and mortality," Eur. J. Orthop. Surg. Traumatol. **25**(1 Suppl 1), S205–S212 (2015).
5. J. Ma, S. Fan, and F. Zhao, "Intraoperative malposition of pedicle probe or screws: a potential cause of the acceleration of degeneration in superior adjacent intervertebral disc," Med. Hypotheses **77**(6), 1102–1104

Biomedical Optics EXPRESS

(2011).
6. N. E. Epstein, "A review of medicolegal malpractice suits involving cervical spine: what can we learn or change?" J. Spinal Disord. Tech. **24**(1), 15–19 (2011).
7. F. M. Phillips, I. Cheng, Y. R. Rampersaud, B. A. Akbarnia, L. Pimenta, W. B. Rodgers, J. S. Uribe, N. Khanna, W. D. Smith, J. A. Youssef, W. A. Sulaiman, A. Tohmeh, A. Cannestra, R. N. Wohns, D. O. Okonkwo, F. Acosta, E. J. Rodgers, and G. Andersson, "Breaking Through the "Glass Ceiling" of Minimally Invasive Spine Surgery," Spine **41**(8 Suppl 8), S39–S43 (2016).
8. M. Vazan, J. Gempt, B. Meyer, N. Buchmann, and Y. M. Ryang, "Minimally invasive transforaminal lumbar interbody fusion versus open transforaminal lumbar interbody fusion: a technical description and review of the literature," Acta Neurochir. (Wien) **159**(6), 1137–1146 (2017).
9. C. L. Goldstein, F. M. Phillips, and Y. R. Rampersaud, "Comparative Effectiveness and Economic Evaluations of Open Versus Minimally Invasive Posterior or Transforaminal Lumbar Interbody Fusion: A Systematic Review," Spine **41**(1 Suppl 8), S74–S89 (2016).
10. C. L. Goldstein, K. Macwan, K. Sundararajan, and Y. R. Rampersaud, "Perioperative outcomes and adverse events of minimally invasive versus open posterior lumbar fusion: meta-analysis and systematic review," J. Neurosurg. Spine **24**(3), 416–427 (2016).
11. V. M. Lu, P. Kerezoudis, H. E. Gilder, B. A. McCutcheon, K. Phan, and M. Bydon, "Minimally Invasive Surgery Versus Open Surgery Spinal Fusion for Spondylolisthesis: A Systematic Review and Meta-analysis," Spine **42**(3), E177–E185 (2017).
12. M. H. Wu, N. K. Dubey, Y. Y. Li, C. Y. Lee, C. C. Cheng, C. S. Shi, and T. J. Huang, "Comparison of minimally invasive spine surgery using intraoperative computed tomography integrated navigation, fluoroscopy, and conventional open surgery for lumbar spondylolisthesis: a prospective registry-based cohort study," Spine J. **17**(8), 1082–1090 (2017).
13. J. H. Oppenheimer, I. DeCastro, and D. E. McDonnell, "Minimally invasive spine technology and minimally invasive spine surgery: a historical review," Neurosurg. Focus **27**(3), E9 (2009).
14. A. Manbachi, R. S. C. Cobbold, and H. J. Ginsberg, "Guided pedicle screw insertion: techniques and training," Spine J. **14**(1), 165–179 (2014).
15. V. Kosmopoulos and C. Schizas, "Pedicle screw placement accuracy: a meta-analysis," Spine **32**(3), E111–E120 (2007).
16. A. Mason, R. Paulsen, J. M. Babuska, S. Rajpal, S. Burneikiene, E. L. Nelson, and A. T. Villavicencio, "The accuracy of pedicle screw placement using intraoperative image guidance systems," J. Neurosurg. Spine **20**(2), 196–203 (2014).
17. V. E. Staartjes, A. M. Klukowska, and M. L. Schröder, "Pedicle Screw Revision in Robot-Guided, Navigated, and Freehand Thoracolumbar Instrumentation: A Systematic Review and Meta-Analysis," World Neurosurg. **116**, 433e8 (2018).
18. T. M. Bydlon, R. Nachabé, N. Ramanujam, H. J. Sterenborg, and B. H. W. Hendriks, "Chromophore based analyses of steady-state diffuse reflectance spectroscopy: current status and perspectives for clinical adoption," J. Biophotonics **8**(1-2), 9–24 (2015).
19. R. Nachabé, B. H. W. Hendriks, A. E. Desjardins, M. van der Voort, M. B. van der Mark, and H. J. Sterenborg, "Estimation of lipid and water concentrations in scattering media with diffuse optical spectroscopy from 900 to 1,600 nm," J. Biomed. Opt. **15**(3), 037015 (2010).
20. R. L. P. van Veen, H. J. Sterenborg, A. Pifferi, A. Torricelli, E. Chikoidze, and R. Cubeddu, "Determination of visible near-IR absorption coefficients of mammalian fat using time- and spatially resolved diffuse reflectance and transmission spectroscopy," J. Biomed. Opt. **10**(5), 054004 (2005).
21. R. Nachabé, J. W. van der Hoorn, R. van de Molengraaf, R. Lamerichs, J. Pikkemaat, C. F. Sio, B. H. W. Hendriks, and H. J. Sterenborg, "Validation of interventional fiber optic spectroscopy with MR spectroscopy, MAS-NMR spectroscopy, high-performance thin-layer chromatography, and histopathology for accurate hepatic fat quantification," Invest. Radiol. **47**(4), 209–216 (2012).
22. B. J. Tromberg, N. Shah, R. Lanning, A. Cerussi, J. Espinoza, T. Pham, L. Svaasand, and J. Butler, "Non-invasive in vivo characterization of breast tumors using photon migration spectroscopy," Neoplasia **2**(1-2), 26–40 (2000).
23. L. Spinelli, A. Torricelli, A. Pifferi, P. Taroni, G. M. Danesini, and R. Cubeddu, "Bulk optical properties and tissue components in the female breast from multiwavelength time-resolved optical mammography," J. Biomed. Opt. **9**(6), 1137–1142 (2004).
24. A. Swamy, G. Burström, J. W. Spliethoff, D. Babic, C. Reich, J. Groen, E. Edström, A. Elmi Terander, J. M. Racadio, J. Dankelman, and B. H. W. Hendriks, "Diffuse reflectance spectroscopy, a potential optical sensing technology for the detection of cortical breaches during spinal screw placement," J. Biomed. Opt. **24**(1), 1–11 (2019).
25. D. C. Karampinos, S. Ruschke, M. Dieckmeyer, M. Diefenbach, D. Franz, A. S. Gersing, R. Krug, and T. Baum, "Quantitative MRI and spectroscopy of bone marrow," J. Magn. Reson. Imaging **47**(2), 332–353 (2018).
26. E. De Bisschop, R. Luypaert, O. Louis, and M. Osteaux, "Fat fraction of lumbar bone marrow using in vivo proton nuclear magnetic resonance spectroscopy," Bone **14**(2), 133–136 (1993).
27. B. Guiu, R. Loffroy, J. M. Petit, S. Aho, D. Ben Salem, D. Masson, P. Hillon, J. P. Cercueil, and D. Krause, "Mapping of liver fat with triple-echo gradient echo imaging: validation against 3.0-T proton MR spectroscopy," Eur. Radiol. **19**(7), 1786–1793 (2009).

Biomedical Optics EXPRESS

28. I. J. MacEwan, N. E. Glembotski, D. D'Lima, W. Bae, K. Masuda, H. H. Rashidi, L. K. Mell, and M. Bydder, "Proton density water fraction as a biomarker of bone marrow cellularity: validation in ex vivo spine specimens," Magn. Reson. Imaging **32**(9), 1097–1101 (2014).
29. W. T. Chen and T. T. F. Shih, "Correlation between the bone marrow blood perfusion and lipid water content on the lumbar spine in female subjects," J. Magn. Reson. Imaging **24**(1), 176–181 (2006).
30. T. Baum, S. P. Yap, M. Dieckmeyer, S. Ruschke, H. Eggers, H. Kooijman, E. J. Rummeny, J. S. Bauer, and D. C. Karampinos, "Assessment of whole spine vertebral bone marrow fat using chemical shift-encoding based water-fat MRI," J. Magn. Reson. Imaging **42**(4), 1018–1023 (2015).
31. A. Régis-Arnaud, B. Guiu, P. M. Walker, D. Krausé, F. Ricolfi, and D. Ben Salem, "Bone marrow fat quantification of osteoporotic vertebral compression fractures: comparison of multi-voxel proton MR spectroscopy and chemical-shift gradient-echo MR imaging," Acta Radiol. **52**(9), 1032–1036 (2011).
32. M. A. Bredella, M. Torriani, R. H. Ghomi, B. J. Thomas, D. J. Brick, A. V. Gerweck, C. J. Rosen, A. Klibanski, and K. K. Miller, "Vertebral bone marrow fat is positively associated with visceral fat and inversely associated with IGF-1 in obese women," Obesity (Silver Spring) **19**(1), 49–53 (2011).
33. X. Li, D. Kuo, A. L. Schafer, A. Porzig, T. M. Link, D. Black, and A. V. Schwartz, "Quantification of vertebral bone marrow fat content using 3 Tesla MR spectroscopy: reproducibility, vertebral variation, and applications in osteoporosis," J. Magn. Reson. Imaging **33**(4), 974–979 (2011).
34. M. Dieckmeyer, S. Ruschke, C. Cordes, S. P. Yap, H. Kooijman, H. Hauner, E. J. Rummeny, J. S. Bauer, T. Baum, and D. C. Karampinos, "The need for T□ correction on MRS-based vertebral bone marrow fat quantification: implications for bone marrow fat fraction age dependence," NMR Biomed. **28**(4), 432–439 (2015).
35. E. Roldan-Valadez, C. Piña-Jimenez, R. Favila, and C. Rios, "Gender and age groups interactions in the quantification of bone marrow fat content in lumbar spine using 3T MR spectroscopy: a multivariate analysis of covariance (Mancova)," Eur. J. Radiol. **82**(11), e697–e702 (2013).
36. G. Gokalp, F. S. Mutlu, Z. Yazici, and N. Yildirim, "Evaluation of vertebral bone marrow fat content by chemical-shift MRI in osteoporosis," Skeletal Radiol. **40**(5), 577–585 (2011).
37. J. M. Patsch, X. Li, T. Baum, S. P. Yap, D. C. Karampinos, A. V. Schwartz, and T. M. Link, "Bone marrow fat composition as a novel imaging biomarker in postmenopausal women with prevalent fragility fractures," J. Bone Miner. Res. **28**(8), 1721–1728 (2013).
38. T. Baum, S. P. Yap, D. C. Karampinos, L. Nardo, D. Kuo, A. J. Burghardt, U. B. Masharani, A. V. Schwartz, X. Li, and T. M. Link, "Does vertebral bone marrow fat content correlate with abdominal adipose tissue, lumbar spine bone mineral density, and blood biomarkers in women with type 2 diabetes mellitus?" J. Magn. Reson. Imaging **35**(1), 117–124 (2012).
39. Y. P. Kim, S. Kannengiesser, M. Y. Paek, S. Kim, T. S. Chung, Y. H. Yoo, C. S. Yoon, H. T. Song, Y. H. Lee, and J. S. Suh, "Differentiation between focal malignant marrow-replacing lesions and benign red marrow deposition of the spine with T2*-corrected fat-signal fraction map using a three-echo volume interpolated breath-hold gradient echo Dixon sequence," Korean J. Radiol. **15**(6), 781–791 (2014).
40. C. Schraml, M. Schmid, S. Gatidis, H. Schmidt, C. la Fougère, K. Nikolaou, and N. F. Schwenzer, "Multiparametric analysis of bone marrow in cancer patients using simultaneous PET/MR imaging: Correlation of fat fraction, diffusivity, metabolic activity, and anthropometric data," J. Magn. Reson. Imaging **42**(4), 1048–1056 (2015).
41. S. B. Reeder, H. H. Hu, and C. B. Sirlin, "Proton density fat-fraction: a standardized MR-based biomarker of tissue fat concentration," J. Magn. Reson. Imaging **36**(5), 1011–1014 (2012).
42. R. Nachabé, B. H. W. Hendriks, M. van der Voort, A. E. Desjardins, and H. J. Sterenborg, "Estimation of biological chromophores using diffuse optical spectroscopy: benefit of extending the UV-VIS wavelength range to include 1000 to 1600 nm," Biomed. Opt. Express **1**(5), 1432–1442 (2010).
43. T. J. Farrell, M. S. Patterson, and B. Wilson, "A diffusion theory model of spatially resolved, steady-state diffuse reflectance for the noninvasive determination of tissue optical properties *in vivo*," Med. Phys. **19**(4), 879–888 (1992).
44. C. M. Jarque and A. K. Bera, "A Test for Normality of Observations and Regression Residuals," Int. Stat. Rev. **55**(2), 163–172 (1987).
45. D. York, N. M. Evensen, M. L. Martinez, and J. De Basabe Delgado, "Unified equations for the slope, intercept, and standard errors of the best straight line," Am. J. Phys. **72**(3), 367–375 (2004).
46. S. B. Reeder, H. H. Hu, and C. B. Sirlin, "Proton density fat-fraction: a standardized MR-based biomarker of tissue fat concentration," J. Magn. Reson. Imaging **36**(5), 1011–1014 (2012).
47. E. N. Marieb and K. Hoehn, *Human Anatomy & Physiology*, 9th ed. (Pearson Education, 2007).
48. R. A. Deyo, D. T. Gray, W. Kreuter, S. Mirza, and B. I. Martin, "United States trends in lumbar fusion surgery for degenerative conditions," Spine **30**(12), 1441–1447 (2005).
49. T. Toyone, T. Ozawa, K. Kamikawa, A. Watanabe, K. Matsuki, T. Yamashita, R. Shiboi, M. Takeuchi, Y. Wada, K. Inada, Y. Aoki, G. Inoue, S. Ohtori, and T. Tanaka, "Subsequent vertebral fractures following spinal fusion surgery for degenerative lumbar disease: a mean ten-year follow-up," Spine **35**(21), 1915–1918 (2010).
50. J. P. Kühn, D. Hernando, P. J. Meffert, S. Reeder, N. Hosten, R. Laqua, A. Steveling, S. Ender, H. Schröder, and D. T. Pillich, "Proton-density fat fraction and simultaneous R2* estimation as an MRI tool for assessment of osteoporosis," Eur. Radiol. **23**(12), 3432–3439 (2013).
51. D. K. Yeung, J. F. Griffith, G. E. Antonio, F. K. Lee, J. Woo, and P. C. Leung, "Osteoporosis is associated with

Biomedical Optics EXPRESS

increased marrow fat content and decreased marrow fat unsaturation: a proton MR spectroscopy study," J. Magn. Reson. Imaging **22**(2), 279–285 (2005).
52. A. V. Schwartz, S. Sigurdsson, T. F. Hue, T. F. Lang, T. B. Harris, C. J. Rosen, E. Vittinghoff, K. Siggeirsdottir, G. Sigurdsson, D. Oskarsdottir, K. Shet, L. Palermo, V. Gudnason, and X. Li, "Vertebral bone marrow fat associated with lower trabecular BMD and prevalent vertebral fracture in older adults," J. Clin. Endocrinol. Metab. **98**(6), 2294–2300 (2013).
53. K. de Cássia Braga Ribeiro and L. P. Kowalski, "APACHE II, POSSUM, and ASA scores and the risk of perioperative complications in patients with oral or oropharyngeal cancer," Arch. Otolaryngol. Head Neck Surg. **129**(7), 739–745 (2003).
54. S. L. Wakely, "The posterior vertebral scalloping sign," Radiology **239**(2), 607–609 (2006).
55. E. R. Westrick and W. T. Ward, "Adolescent idiopathic scoliosis: 5-year to 20-year evidence-based surgical results," J. Pediatr. Orthop. **31**(1 Suppl), S61–S68 (2011).
56. S. Ruschke, A. Pokorney, T. Baum, H. Eggers, J. H. Miller, H. H. Hu, and D. C. Karampinos, "Measurement of vertebral bone marrow proton density fat fraction in children using quantitative water-fat MRI," MAGMA **30**(5), 449–460 (2017).
57. T. Baum, A. Rohrmeier, J. Syväri, M. N. Diefenbach, D. Franz, M. Dieckmeyer, A. Scharr, H. Hauner, S. Ruschke, J. S. Kirschke, and D. C. Karampinos, "Anatomical Variation of Age-Related Changes in Vertebral Bone Marrow Composition Using Chemical Shift Encoding-Based Water-Fat Magnetic Resonance Imaging," Front. Endocrinol. (Lausanne) **9**, 141 (2018).
58. S. Merritt, G. Gulsen, G. Chiou, Y. Chu, C. Deng, A. E. Cerussi, A. J. Durkin, B. J. Tromberg, and O. Nalcioglu, "Comparison of water and lipid content measurements using diffuse optical spectroscopy and MRI in emulsion phantoms," Technol. Cancer Res. Treat. **2**(6), 563–569 (2003).
59. G. Burström, R. Nachabe, O. Persson, E. Edström, and A. E. Terander, "Augmented and Virtual Reality Instrument Tracking for Minimally Invasive Spine Surgery: A Feasibility and Accuracy Study," Spine (2019) (published online ahead of print June 12, 2019).
60. M. J. Tormenti, D. B. Kostov, P. A. Gardner, A. S. Kanter, R. M. Spiro, and D. O. Okonkwo, "Intraoperative computed tomography image-guided navigation for posterior thoracolumbar spinal instrumentation in spinal deformity surgery," Neurosurg. Focus **28**(3), E11 (2010).
61. A. Elmi-Terander, G. Burström, R. Nachabe, H. Skulason, K. Pedersen, M. Fagerlund, F. Ståhl, A. Charalampidis, M. Söderman, S. Holmin, D. Babic, I. Jenniskens, E. Edström, and P. Gerdhem, "Pedicle Screw Placement Using Augmented Reality Surgical Navigation With Intraoperative 3D Imaging: A First In-Human Prospective Cohort Study," Spine **44**(7), 517–525 (2019).
62. D. P. Devito, L. Kaplan, R. Dietl, M. Pfeiffer, D. Horne, B. Silberstein, M. Hardenbrook, G. Kiriyanthan, Y. Barzilay, A. Bruskin, D. Sackerer, V. Alexandrovsky, C. Stüer, R. Burger, J. Maeurer, G. D. Donald, R. Schoenmayr, A. Friedlander, N. Knoller, K. Schmieder, I. Pechlivanis, I.-S. Kim, B. Meyer, and M. Shoham, "Clinical acceptance and accuracy assessment of spinal implants guided with SpineAssist surgical robot: retrospective study," Spine **35**(24), 2109–2115 (2010).
63. J. P. Du, Y. Fan, Q. N. Wu, D. H. Wang, J. Zhang, and D. J. Hao, "Accuracy of Pedicle Screw Insertion Among 3 Image-Guided Navigation Systems: Systematic Review and Meta-Analysis," World Neurosurg. **109**, 24–30 (2018).
64. A. Ghasem, A. Sharma, D. N. Greif, M. Alam, and M. A. Maaieh, "The Arrival of Robotics in Spine Surgery: A Review of the Literature," Spine **43**(23), 1670–1677 (2018).